


**Emergence of chimeras: An impetus by exceptional points**M. Paul Asir <sup>\*</sup>*Chennai Institute of Technology, Chennai 600029, India*

(Received 13 April 2023; accepted 7 August 2023; published 22 August 2023)

A nonconservative system with nonreciprocal interaction has been found to reveal exotic features where sudden phase transitions can occur. In this paper, the emanation of a chimera in a network of Stuart-Landau oscillators with nonreciprocal interaction is reported. Note that the spins follow the random discrete distribution. In other words, we pick a random oscillator to rotate clockwise or anticlockwise. At the transition points, we find the spectral singularities in the eigenplane, where eigenvalues coalesce, commonly known as *exceptional points*. We find that the counterrotational symmetry breaking induced by exceptional points antecedents the occurrence of the chimera. We numerically attest to the findings for two cases of initial conditions, namely, bipartite and random. We also extend our study to a two-dimensional array of nonreciprocally interacting, distributed spins. The findings could have pragmatic implications in the areas of active matter, networks, and photonics.

DOI: [10.1103/PhysRevE.108.024220](https://doi.org/10.1103/PhysRevE.108.024220)**I. INTRODUCTION**

The collective behavior of agents that alter their state according to neighbors is of paramount significance [1–5]. Such systems scale from the hydrodynamics of microorganism swarming [6], flocking of birds [7,8], to human social interactions [9,10]. The description of the emergence of collective phenomenon roots from statistical physics, though the local interactions may not resemble the Ising spin. The *correlation* between the organisms plays a key role in the organization of the cluster dynamics. Apart from the clusters that arise in complex networks where diffusion is the caveat, the *nonreciprocal* interaction enforces pattern formation where asymmetric long-range interactions are the key [11]. For instance, plant-animal mutualistic networks [12,13], or an epitome of olfactory receptor neurons in *Drosophila* [14] manifest interactions that are not symmetric. In the above biological models, the system converges to a homogeneous solution, while only nodal interactions are taken into account. Despite this, heterogeneous solutions spontaneously emerge in the presence of long-range interactions among the units. Also, nonreciprocity prevails in active systems that arise in physics, biology, and the social sciences [15–17]. It can be realized through synthetic physical interactions [18], leader-follower relations [19], or programmable robotic interactions [20,21].

A non-Hermitian ( $\mathcal{H} \neq \mathcal{H}^\dagger$ ) matrix arises in a model where the units interact with their environment. The existence of non-Hermitian  $\mathcal{H}$  in a nonreciprocal interaction has been reported recently [22–24]. Non-Hermiticity leads to the spontaneous breaking of time translational symmetry that enforces pattern formation in the model. A  $\mathcal{PT}$ -symmetric Hamiltonian undergoes a further phase transition to the steady state in time (time crystals) as a function of parameter variation

due to the non-Hermitian nature of the stability matrix. The stability of the phases is determined by evaluating the eigenmodes of  $\vec{\mathcal{J}}$ . If the perturbations become undamped yet the growth rate  $\sigma_i$  becomes close to zero, this signifies the phase transition to the chiral phase. At this point, the spectrum of the eigenvalues *coalesce*, termed as *exceptional points* [25–27]. More generally, exceptional transitions can be viewed as the dynamical restoration of a spontaneously broken continuous symmetry: the steady state is actuated by the parameter variation, and after the transition, the system runs along the manifold of degenerate ground states. Exceptional points commonly indicate the transition between traveling or oscillatory solutions and exponentially decaying dynamics. The nonmutual or nonreciprocal interactions that foster the splitting and merging of dynamical states often coincide with the coalescence of Lyapunov covariant vectors, which marks the generalization of exceptional points in nonlinear dynamics [28]. Conspicuously, in photonic systems, optical gain and loss modes manifest the emergence of exceptional points that dramatically alter the cumulative effect, leading to a range of exotic functionalities associated with abrupt phase transitions in the eigenvalue spectrum [29]. Lately, non-Hermitian degeneracy has also been used for the design of laser systems, new nonlinear optics phenomena, and scattering features in open systems. Significantly, a magnetic bilayer with unidirectional coupling was shown to exhibit electrically actuated spin-current transmission, and unidirectional spin-wave packet generation and propagation [30].

Conversely, a well-established notion of collective dynamics in diffusive networks, namely, the *chimeras*, has been found in many complex networks [31–35]. Also, in certain models, a transition to a steady state has been encountered in the chimeric regime, termed chimera death. Due to the interplay of nonlocality and the breaking of rotational symmetry by the coupling, an abrupt transition from chimeric oscillations to a steady state has been noticed [36–38]. A two-level synchronization mechanism has been found to give

<sup>\*</sup>Corresponding author: paulphy.asir@gmail.com

rise to the chimera in a two-frequency model where sequential alternation of synchronized and asynchronous domains exists. As the system evolves, the frequency  $\omega_i$  of each oscillator will poise towards one of the two attracting fixed points depending on their initial conditions. At the borders of two-frequency domains, asynchronous oscillations persist [39].

Motivated by the above facets, we interrogate whether chimeras can arise through exceptional points (EPs) in a network with nonreciprocal interaction. In this study, we extrapolate the origin of chimera with the impetus of EPs. Analogous to the non-Hermitian degeneracies, we find a counterrotational symmetry-breaking mechanism inducing chimeric patterns in a network with asymmetric interaction. At that point of symmetry breaking, we detect spectral singularities in the eigenplane. Notably, we find an intriguing state where the collective state of a network consists of coherent, incoherent, and damped state, which we coin as *demonic chimera* (DC). We chose a network of Stuart-Landau oscillators with clockwise and anticlockwise rotations distributed in a specific way to affirm the presence of the chimeric patterns. Also, we investigate a two-dimensional (2D) array of oscillators with nonreciprocal interaction.

The organization of the paper is as follows. Section II presents the model description along with a stability analysis. Section III discusses the results of the numerical simulations. Section IV summarizes the findings with a conclusion.

## II. GOVERNING EQUATION

The general form of the network with nonreciprocal interaction is written as

$$\dot{\mathbf{X}}_i = F(\mathbf{X}_i) + \epsilon_1 \mathbf{X}_j - \epsilon_2 \mathbf{X}_j, \quad (1)$$

where  $\mathbf{X}_i = [x_1, x_2, x_3, \dots, x_N]^T \in \mathcal{R}^N$  is the matrix representing the individual states of the oscillator.  $F(\cdot)$  denotes a nonlinear function that defines the rule of evolution. Note that the sign of interaction for either  $\pm$  rely on the frequency of the  $i$ th oscillator. A pair of oscillators can have a attraction or level of repulsion based on the angular frequency of the  $i$ . We choose  $N = 120$ .

As an high point, we take a network of nonlinear oscillating equations near the supercritical Hopf bifurcation, namely, the Stuart-Landau (SL) model. The SL dynamical model is first introduced to analyze the transition to turbulence in a plane Poissuille flow [40,41]. The hydrodynamic stability varies with the magnitude of the disturbance. Precisely, the complex growth rate  $\sigma + i\omega$  determines the hydrodynamic stability.

Due to the ubiquity of the equation, it finds potential significance in fluid dynamics [42], Belusov-Zabotinsky [43] reactions, and so on. The  $\dot{z}_j = f(z_j)$  presents the complex form for the SL equation with the local  $j = 1, \dots, N$  deterministic dynamics is given by [44]

$$f(z_j) = (A + i\omega - |z_j|^2)z_j, \quad (2)$$

where  $z_j = x_i + iy_i = r_j e^{i\phi_j} \in \mathbb{C}$ , with  $x_i, y_i \in \mathbb{R}$ . A single SL oscillator exhibits self-sustaining oscillations with frequency  $\omega$  and radius  $r_j = \sqrt{A}$ . A network of SL oscillators with nonreciprocal interaction in Cartesian form can be laid out as

$$\begin{aligned} \dot{x}_i &= (A - x_i^2 - y_i^2)x_i - \omega_i y_i - \epsilon_1 \mathcal{G}(\omega)x_j + \epsilon_2 [1 - \mathcal{G}(\omega)]x_j, \\ \dot{y}_i &= (A - x_i^2 - y_i^2)y_i + \omega_i x_i, \end{aligned} \quad (3)$$

where  $A$  is the amplitude of the disturbance,  $\omega_i$  is the angular frequency of the  $i$ th oscillator. Note that we fix  $\omega_i = \pm 1$  based on a specific distribution. We remark that  $\omega = 1$  denotes the clockwise rotation and  $\omega = -1$  is for the anticlockwise rotation. The attractive or repulsive interaction between the nearest neighbors has been doomed by  $\omega_i$ . The discrete scaling function  $\mathcal{G}(\omega)$  is given by

$$\mathcal{G}(\omega) = \begin{cases} 0, & \omega_i = -1, \\ 1, & \omega_i = 1. \end{cases} \quad (4)$$

We pick a random discrete distribution of  $\omega_i$ . We numerically study the two cases of initial conditions and the associated behavior. In case I, the bivariate initial conditions and in case II, purely random initial conditions. The stability analyses for the two coupled oscillators are given below. The *singular* exceptional points are given by

$$\begin{aligned} x_1^* &= -\omega_1 - \epsilon_1 - \omega_1^2(A - \omega_1 - \epsilon_1), \\ y_1^* &= \pm\sqrt{A - \omega_1 - \epsilon_1}, \\ x_2^* &= -\omega_2 - \epsilon_2 - \omega_2^2(A - \omega_2 - \epsilon_2), \\ y_2^* &= \pm\sqrt{A - \omega_1 - \epsilon_2}, \end{aligned} \quad (5)$$

and the *parity symmetric* exceptional points are

$$\begin{aligned} x_1^* &= \sqrt{-2\omega_1 - \epsilon_1}, \\ y_1^* &= \pm\sqrt{-A + 2\omega_1 - \epsilon_2 - \omega_1}, \\ x_2^* &= \sqrt{2\omega_2 + \epsilon_2}, \\ y_2^* &= \sqrt{A + 2\omega_1 + \epsilon_1 + \omega_2}. \end{aligned} \quad (6)$$

The stability determining matrix of the two coupled oscillators can be written as

$$\vec{\mathcal{J}} = \begin{bmatrix} A - 3x_1^2 - y_1^2 - \omega_1 & -2y_1x_1 - \lambda & -\epsilon_1 & 0 \\ -2x_1y_1 - \lambda & A - 3y_1^2 & 0 & 0 \\ \epsilon_2 & 0 & A - 3x_2^2 - y_2^2 - \omega_2 - \lambda & -2x_2y_2 \\ 0 & 0 & -2x_2y_2 & A - x_2^2 - 3y_2^2 - \omega_2 - \lambda \end{bmatrix}. \quad (7)$$

At  $\lambda = 0$ , the critical transition point is derived as

$$\begin{aligned} \epsilon_1 &= A - 3x_1^2 - y_1^2 - \omega_1 [A - 3y_1^2(A - 3x_2^2 - y_2^2 - \omega_2)(A - x_2^2 - 3y_2^2 - \omega_2) - (2x_2y_2)^2] \\ &\quad - (2x_1y_1)^2(A - 3x_2^2 - y_2^2 - \omega_2)(A - x_2^2 - 3y_2^2 - \omega_2) - (2x_2y_2)^2 / [A - 3y_1^2(A\epsilon_2 - x_2^2 - 3y_2^2 - \omega_2)]. \end{aligned} \quad (8)$$

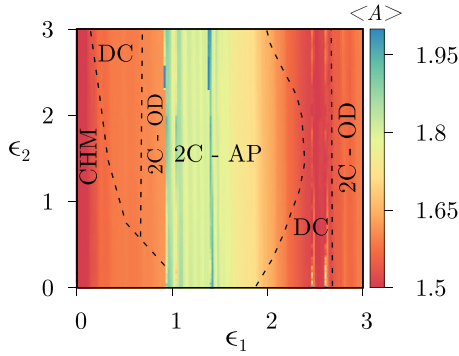


FIG. 1. Empirical numerical estimate of the parameter space in the  $\epsilon_1$ - $\epsilon_2$  plane. Note that the initial conditions are bipartite. A series of complex collective phenomena as a function of coupling strengths are shown. The transition from chimeras to demonic chimeras to 2C-oscillation death occurs due to the breaking of rotational symmetry. We see a midregion of space where nodes aligned as a two cluster antiphase synchronized states. The dotted lines are an approximate estimation of the boundaries that separates each distinct region.

### III. NUMERICAL STUDY

We perform a numerical simulation of Eq. (2) with Runge-Kutta  $\mathcal{O}(4)$  with the fixed  $\Delta t = 0.01$ . The nonreciprocal interaction with random *spins* is found to induce intriguing chimeras due to the breaking of rotational symmetry at exceptional points. The role of initial conditions on the resultant chimeric patterns has been widely investigated.

#### A. Case I: Bipartite initial conditions

We choose  $x_0, y_0 > 0$  for  $N/2$ , and the next half of the oscillators in networks start in the negative quadrant  $x_0, y_0 < 0$ . We compute the empirical parameter space with an order parameter that averages the amplitude of each node  $i$ , Fig. 1. The order parameter  $\langle A \rangle = \frac{1}{N} \sum_{i=1}^N \{ \frac{1}{T} \int_0^T x_i(t) dt \}$ . Based on the range of averages, we classify the regions into different dynamical regimes. Note that the frequencies  $\omega_i$  follow a discrete random distribution. The parameter space is computed with 50 different sets of initial conditions, and the mean of the order parameter is taken into account. In the  $\epsilon_1 - \epsilon_2$  parameter plane, we found chimeras (CHM), demonic chimeras (DC), two-cluster parity-symmetric states (2C-OD), and two-cluster antiphase synchronized states (2C-AP). The dotted lines are laid out numerically to have rough boundaries between dynamic regimes. We see that there is a clear phase transition from chimera to demonic chimera (DC) to 2C-OD in  $0 < \epsilon_1 < 1$ . We find that this transition occurs through the breaking of the rotational symmetry of the nearest neighbors. Initial conditions play a key role in achieving these states. The inertia of the  $i$ th oscillator pulls the  $i + 1$  towards alignment due to  $+\epsilon x_j$ . In contrast, the level repulsion induced by  $-\epsilon x_j$  pushes the adjacent oscillators away from each other. Hence, spins with closely related phases club together to form synchronized clusters, while those that start apart diverge to produce incoherent regimes. We notice an interesting state between the chimera and 2C-OD states, where coherent, incoherent, and nonoscillatory states coexist in space for a

particular value of nonreciprocity. We coin this state as “demonic chimera.” At some region of  $1 < \epsilon_1 < 2$ , two clusters of antiphase synchronization persist where the oscillators antialign with each other. Note that we find a multiclustered antiphase synchronized state. The boundary between distinct states is marked by exceptional points. These EPs induce the breaking of rotational symmetry that causes the phase transition among different states. We observe that these phenomena are initial phase-dependent states induced by nonreciprocity. From the perspective of EPs, the coalescence of eigenmodes induces this sort of transition. The order parameter  $\langle A \rangle$  falls into a certain bin for each ordered and disordered phase. The critical eigenvalue spectrum within the parameter regime is found to be linearly independent  $\lambda_1 = \lambda_2$  marks the presence of EPs. The nonreciprocal interaction thus ensures nonorthogonality of eigenmodes, i.e., the eigenvalues are parallel at the transition points. The eigenvalues of linearized  $\vec{J}$  equals  $\lambda = \sigma + i\omega$ , and involves both the growth rate and frequencies. Also, the real part of the eigenvalue, which dictates the growth rate of  $\sigma$ , is close to zero in a damped state. In non-Hermitian quantum mechanics, these transitions are supposed to be poised towards spontaneous  $\mathcal{PT}$  symmetry breaking. The dynamic restoration of the damped state is ensured by the spontaneous parity symmetry formation with the variation in parameter.

We extracted distinct dynamical regimes from the parameter space, Fig. 1 and presented them in Fig. 2. The relevant spatiotemporal patterns, snapshots, and polar plots of the  $i$ th phase at an instant of time are presented in a row. Figure 2(a) shows the chimeric patterns that involve the coexistence of distinct synchronized and incoherent regimes at  $\epsilon_1 = 0.1$ ,  $\epsilon_2 = 0$ . Note that the bipartite initial conditions favor the clustering of counterregimes. Due to the randomness involved in the distribution of  $\omega_i$ , we see intermittent phase slips in the synchronized domain. The snapshot and the polar plot reveal the coexistence of ordered and disordered phases. In Fig. 2(b), at  $\epsilon_1 = 0.3$  and  $\epsilon_2 = 2$ , a distinguished pattern of concurrent presence of incoherent, coherent, and strips of damped regions manifests the DC. We find the prevalence of this dynamic near the transition to a parity symmetric state. The dynamic restoration as a function of a parameter near the edge of transition to a damped state is responsible for the occurrence of DC. Figure 2(c) shows the emergence of a parity symmetric damped state at  $\epsilon_1 = 1.5$  and  $\epsilon_2 = 2$ . Also, we infer that the counterpropagation of phases along the network causes rotational asymmetry and leads to a damped state.

Next, we compute the autocorrelation index (CI) of the neighboring nodes  $C_{ij}(\langle A \rangle)$ . Explicitly,  $C_{ij}(\langle A \rangle) = |\langle A_i \rangle - \langle A_{i+1} \rangle|$ . The measure reveals the correlation of the amplitudes that appear in distinct patterns. The identical adjacent points mark the degree of synchronization between the nodes, Fig. 3. If  $i$  and  $i + 1$  are completely synchronized then  $C_{ij}(\langle A \rangle) = 1$ , otherwise they are scaled by a fraction. The CI at  $\epsilon_1 = \epsilon_2 = 0$  shows the characteristics of incoherence by displaying dissimilar adjacent points (blue line with dots). The region at which  $C_{ij}(\langle A \rangle) = 0$  denotes complete incoherence. At  $\epsilon_1 = 0.3$  and  $\epsilon_2 = 0.5$ , we find two-cluster antiphase synchronizations. The erratic behavior in the CI profile is evident from Fig. 3(a) (olive green line with dots). The adjacent oscillators

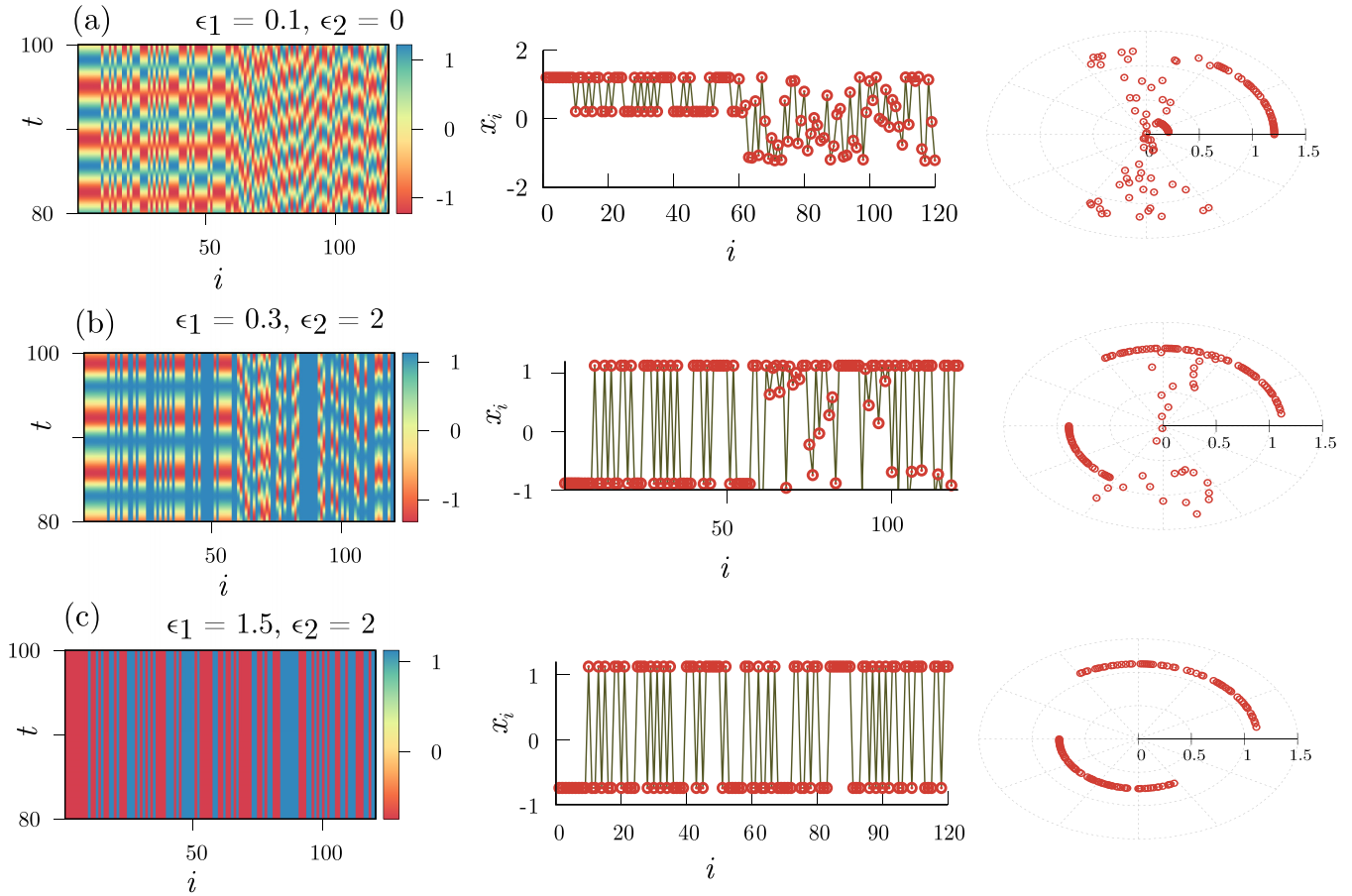


FIG. 2. Note that the initial conditions are bipartite. A series of complex collective phenomena as a function of coupling strengths are shown. Rows distinctly decipher the states at a particular parameter through spatiotemporal patterns, snapshots, and Polar plots (from left to right). (a) Row depicts the chimera state at  $\epsilon_1 = 0.1, \epsilon_2 = 0 \mapsto$  chimera. (b)  $\epsilon_1 = 0.3, \epsilon_2 = 2 \mapsto$  demonic chimera. (c)  $\epsilon_1 = 1.5, \epsilon_2 = 2 \mapsto$  2 cluster damped state.

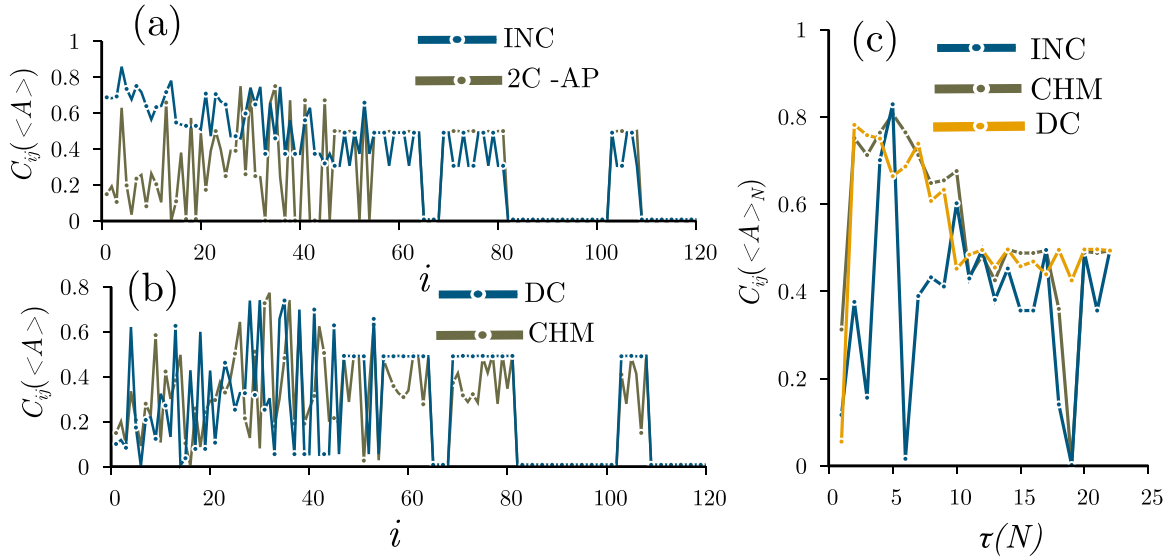


FIG. 3. (a) Autocorrelation index between adjacent average amplitudes of the oscillators  $\langle A \rangle$  in a network with  $N = 120$ . We choose initial conditions distributed into two halves of  $N$  with opposite signs. The blue and the olive dotted lines represents the  $C_{ij}(\langle A \rangle)$  of the incoherent (INC) and two-cluster antiphase synchronized states (2C-APS) in a network. The zero auto-correlation index indicates exactly the complete incoherence. The coupling strengths leads to attraction and level repulsion in the Riemann’s surface of eigenvalue plane are denoted as  $\epsilon_1 = 0, \epsilon_2 = 0$  for incoherent domain. The  $\epsilon_1 = 0.3, \epsilon_2 = 0.5$  two cluster antiphase synchronized states (2C-APS). (b)  $\epsilon_1 = 0.3, \epsilon_2 = 2$  for demonic chimera (DC) states (blue lines with dots).  $\epsilon_1 = 0.1, \epsilon_2 = 0$  for chimera (CHM). (c) The autocorrelation index  $C_{ij}(\langle A \rangle_N)$  for  $\langle A \rangle$  with an increase in  $N$ . The  $\tau(N)$  indicates the interval to obtain correlation in  $N$ .



do not align exactly opposite to each other, but the overall index averages to  $C_{ij}(\langle A \rangle) = 0.5$ . For  $i > 80$ , most of the oscillators align exactly at opposite phases. The amplitude correlation of DC at  $\epsilon_1 = 0.3$ ,  $\epsilon_2 = 2$  is shown in Fig. 3(b). Uniform points in the interval of  $65 \leq i \leq 80$  indicate a stable damped regime. While the initial nodes of the network displaying lesser CI disseminate incoherence. In the interval  $20 < i < 60$ ,  $C_{ij}(A) \simeq 0.8$  shows the coherent regime. Also, the CI profile of the chimera is shown at  $\epsilon_1 = 0.1$  and  $\epsilon_2 = 0$ .

Further, we trace the evolution of the amplitude correlation index as a function of the number of the oscillators in a network. The ordinate denotes the correlation delay  $\tau(N)$ , Fig. 3(c). We find that, with an increase in the  $\tau(N)$ , the  $C_{ij}(\langle A \rangle_N)$  averages to half. In an incoherence regime, the correlation index occupies lower values. However, long-range correlations are approximately 0.5. The chimeric pattern autocorrelation index  $C_{ij}(\langle A \rangle_N) > 0.5$  is due to the presence of coherent regimes. The long-range correlation is almost similar to the incoherent regimes due to the coexistence of ordered and disordered states. Analogous to chimeras, the DC also exhibits a decay of long-range correlation. We explore the mechanism behind the emergence of chimeras through exceptional points, Fig. 4. The bifurcation of two coupled oscillators with opposite spins as a function of  $\omega_1 \in [-1, 1]$  is plotted in Fig. 4(a). We fix  $\omega_2 = 1$ . We wish to excavate the role of rotational asymmetry coincident with exceptional points in influencing the transition to chimeras. We fix the interaction strengths,  $\epsilon_1 = 0.05$  and  $\epsilon_2 = 0.0$ . The forward and backward continuation bifurcations display discontinuity due to the singularities present in the eigenplane. We claim that, at that interval of space, the exceptional point emerges, which pivots the breaking of counterrotational symmetry that leads to chimeric patterns. We also calculate the expectation value of the energy given by

$$\langle E \rangle = \frac{1}{T} \int_0^T X_i(\omega) X_j(\omega) \Lambda_{ij}, \quad (9)$$

where  $\Lambda_{ij} = \frac{1}{i} \ln \left| \frac{dF}{dx} \right|_{x=x^*}$  is the covariant Lyapunov eigenvalues. Figure 4(b) shows a codimension of two bifurcations in the  $\omega_1$ - $\omega_2$  plane. The estimated  $\langle E \rangle$  possesses singularity at the point of transition seen from the white space on the map shown at the top. We find that the eigenvalues at these points possess a signature of coalescence, i.e.,  $\lambda_1 = \lambda_2$ . At the exceptional point, counterrotational symmetry breaks, which leads to the dynamical restoration of parity symmetry. Also, the nonreciprocal interaction ensures the nonorthogonality of eigenvectors that enables the spontaneous  $\mathcal{PT}$ -symmetric breaking. After the exceptional transition, the spins align together to form coherent and incoherent clusters that give birth to chimeras. Near the exceptional points, antiphase and chimeric clusters exhibit finite wavelength instability in the transverse direction. The eigenvalues in the vicinity of an exceptional point behave as  $s = \pm i\sqrt{\Delta}$ , where  $\Delta$  is a characteristic distance from the exceptional point. Typically,  $s = \pm \sigma + i\omega$ , where at-least one of the  $\sigma$  has a positive real part, causing instability. The demonic chimeras also arise as a consequence of parity symmetry at the edge of the transition to damped mode. To trace the evolution of exceptional points, we

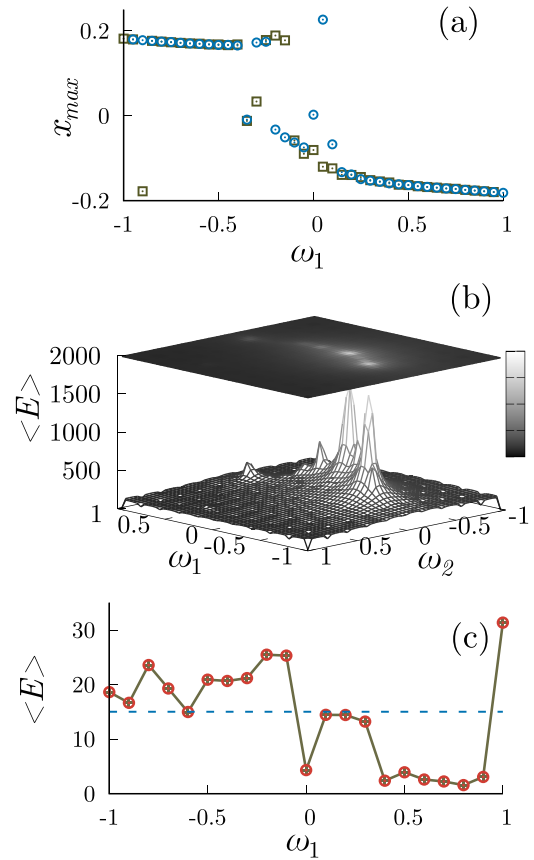


FIG. 4. (a) Forward and backward bifurcation plots in the  $\omega_1 - x_{max}$  plane. Note that we fix  $\omega_2 = 1$ . The singularities can be found near  $\omega_1 \approx 0$  where the exceptional points lie. (b) Two-parameter plot depicting the mean energy  $\langle E \rangle$  fluctuations in the fabric. The top layer shows the density of  $\langle E \rangle$ . Note that the light spots denote the exceptional points where eigenvalues coalesce. (c)  $\omega_1$  versus  $\langle E \rangle$  with fixed  $\omega_2 = 1$ ,  $\epsilon = 2$ ,  $\epsilon = 1.5$ . The points above the blue line correspond to exceptional points.

calculate the energy as a function of  $\omega_1$  with a fixed  $\omega_2 = 1$ . The blue line denotes the  $\langle E \rangle$  above which exceptional points arise. We see that with the fixed  $\omega_2$ , most of the EPs lie in the negative quadrant.

## B. Case II: Random initial conditions

Next, we move on to investigate the role of pure random initial conditions on the exceptional points that enforce pattern formation. We find an incoherent state at  $\epsilon_1 = \epsilon_2 = 0$  as shown in Fig. 5(a). The corresponding random distribution of phases in the snapshot and polar plot prove the state. With a further increase in coupling strength to  $\epsilon_1 = 2$  and  $\epsilon_2 = 2.1$ , we observe multicluster synchronized regimes located among incoherent phases. This shows the existence of chimeric patterns, Fig. 5(b). Due to the randomness in the distribution of the initial phases and frequencies, the number of clusters or the site at which they appear will alter with every iteration. Also, we evince the existence of demonic chimera where oscillation states with order and disordered and damped regimes coexist at  $\epsilon_1 = 2.5$  and  $\epsilon_2 = 2$ . In Fig. 5(c) we trace the strips of nonoscillatory parity-symmetric states along with

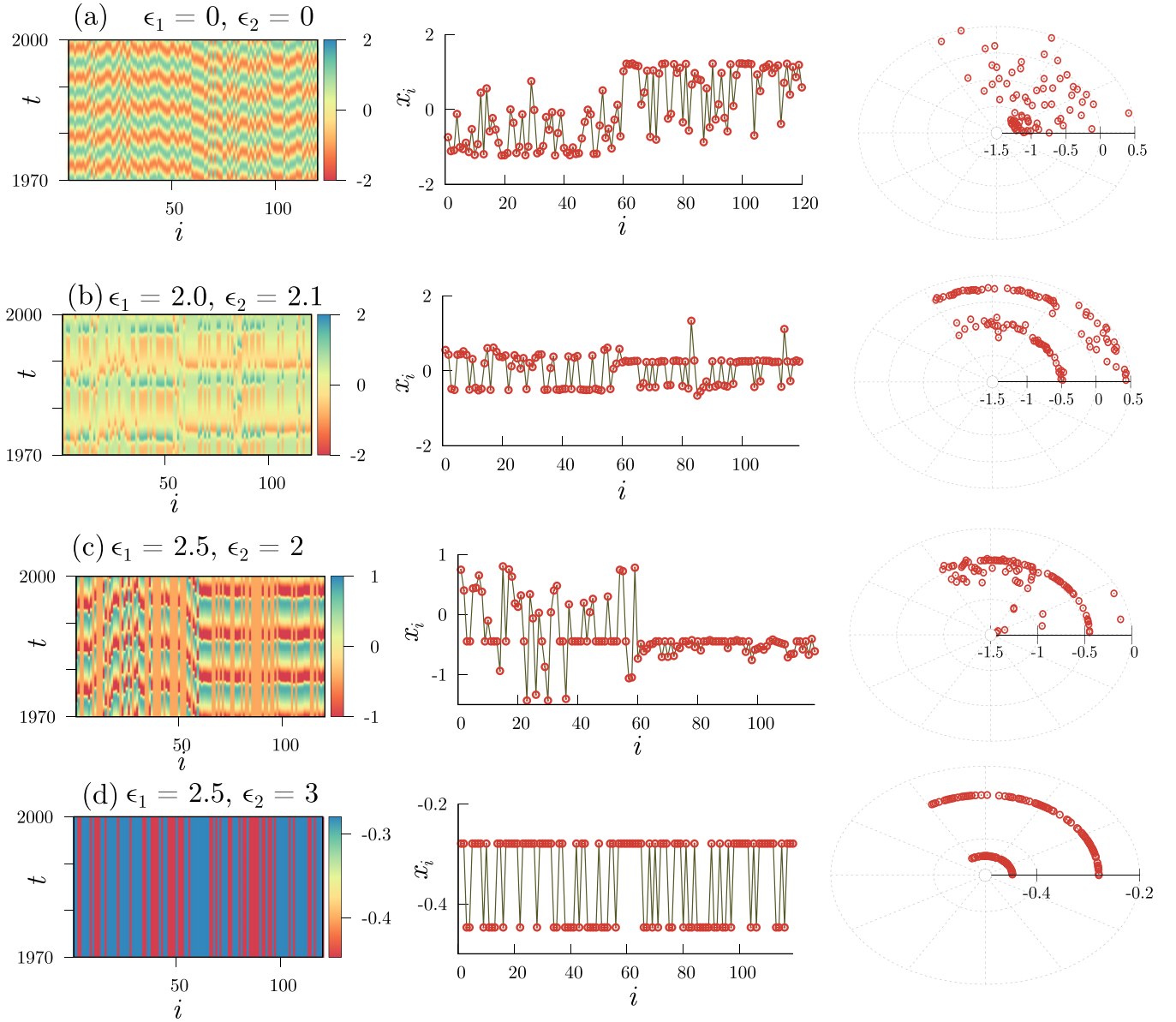


FIG. 5. Note that the initial conditions are random. A series of complex collective phenomena as a function of coupling strengths are shown. Columns distinctly decipher the states at a particular parameter through spatiotemporal patterns, snapshots, and Polar plots (from left to right). (a) Row depicts the incoherence state at  $\epsilon_1 = \epsilon_2 = 0$ . (b)  $\epsilon_1 = 2.0, \epsilon_2 = 2.1 \mapsto$  chimera. (c)  $\epsilon_1 = 2.5, \epsilon_2 = 2 \mapsto$  demonic chimera. (d)  $\epsilon_1 = 2.5, \epsilon_2 = 3 \mapsto$  2 cluster OD state.

coherent and incoherent regimes. Upon further increasing the  $\epsilon_1 = 2.5$  and  $\epsilon_2 = 3$ , we find a completely damped state with two distinct clusters arising due to the dynamic restoration of the parity symmetric state, Fig. 5(d).

As in the previous case, we study the amplitude correlation characteristics of the distinct patterns found in Eq. (3) with random initial conditions. Figure 6(a) shows the correlation index of the two cluster antialigned and DC states. The periodic switching of  $C_{ij}(\langle A \rangle)$  between two values indicates the presence of two distinctly aligned phases. Also, the demonic chimera states at  $\epsilon_1 = 2.5$  and  $\epsilon_2 = 2.0$  can be referred to from the identical  $C_{ij}(\langle A \rangle)$  of adjacent nodes for  $i > 60$ . It shows the presence of coherent oscillatory and damped states. Note that the ergodic correlation index for  $i < 60$  is due to

randomness in initial phases. At a null value of interaction strength  $\epsilon_1 = \epsilon_2 = 0$ , the incoherence is identified from the elevated CI. From Fig. 6(b), randomly aligned incoherent phases and coherent clusters can be identified from the corresponding CI at  $i < 60$  and  $i > 80$ . Note that  $C_{ij}(\langle A \rangle)$  shows an identical correlation index near  $i \simeq 100$ .

We study the long-range amplitude correlation index of distinct dynamical patterns as a function of  $\tau(N)$ , Fig. 6(c). With an increase in  $\tau(N)$  the  $C_{ij}(\langle A \rangle_N)$  asymptote to a constant value. We find an exponential decay of the correlation index as the correlation distance increases. Demonic chimeras shows a similar pattern but with an elevation in the tail. Obviously, for incoherence  $C_{ij}(\langle A \rangle_N) > 0.5$ , yet suffers a mild decay as  $\tau(N)$  grows.

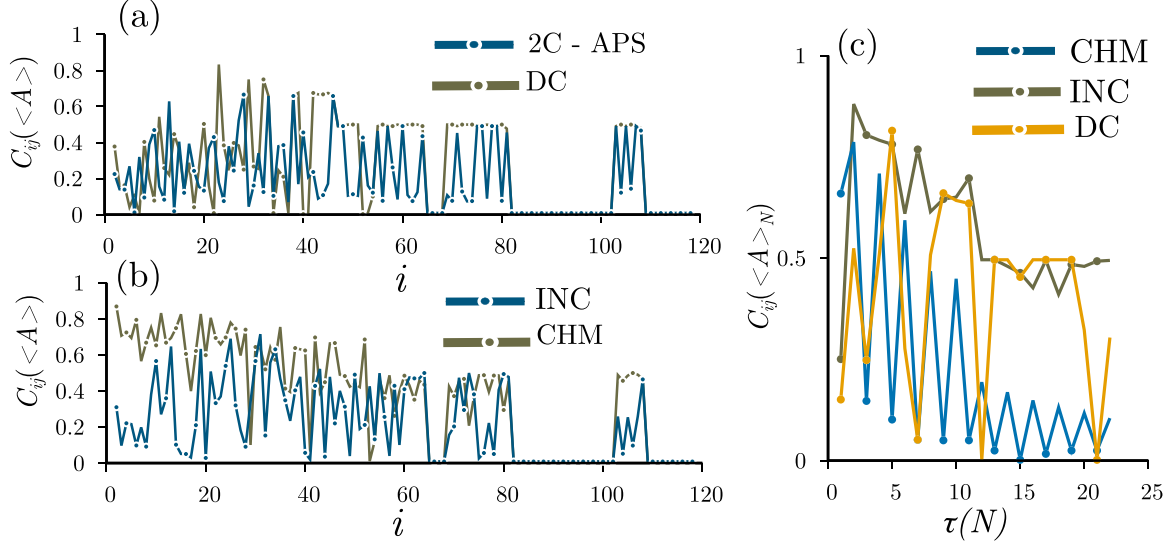


FIG. 6. (a) Autocorrelation index between adjacent average amplitudes of the oscillators  $\langle A \rangle$  in a network with  $N = 120$ . We choose initial conditions *randomly* distributed into two halves of  $N$  with opposite signs. The blue and the olive dotted lines represents the  $C_{ij}(\langle A \rangle)$  of the two-clustered antiphase synchronization (2C-APS) and complete incoherence (INC) in a network. The zero autocorrelation index indicates exactly the opposite phases of adjacent oscillators. The coupling strengths leads to attraction and level repulsion in the Riemann's surface of eigenvalue plane are denoted as  $\epsilon_1 = 0.5, \epsilon_2 = 0.35$  for 2C-APS. The  $\epsilon_1 = 2.5, \epsilon_2 = 2.0$  for demonic chimera (DC). (b)  $\epsilon_1 = 0, \epsilon_2 = 0$  for incoherent domain (blue lines with dots).  $\epsilon_1 = 2, \epsilon_2 = 2.1$  for chimera (CHM). (c) The autocorrelation index  $C_{ij}(\langle A \rangle_N)$  for  $\langle A \rangle$  with an increase in  $N$ . The  $\tau(N)$  indicates the interval to obtain correlation in  $N$ .

#### IV. CHIMERAS IN NONRECIPROCAL NETWORK: 2D ARRAY

Higher-dimensional chimera states are particularly astonishing due to their prevalence in the fields of optics [45], phase oscillators [46], superconducting quantum interference device (SQUID) metamaterials [47], and so on. In addition, spiral wave chimeras have been found in a 2D array of nonlocally

coupled Belusov-Zhabotinsky reactions [48]. These spirals with an asynchronous center surrounded by synchronous clusters have been found to occur in SQUID metamaterials [49], cortical tissues [50], cilia carpets [51], and optomechanical microresonators [52]. We study the emergence of chimera states in a 2D array of Eq. (3) with nonreciprocal interaction. The equations of motion in a 2D array can be written as

$$\begin{aligned}
 \dot{x}_{i,j} &= (A - x_{i,j}^2 - y_{i,j}^2)x_{i,j} - \omega_i y_{i,j} - \epsilon_1 \mathcal{G}(\omega)[x_{i+1,j} + x_{i-1,j} + x_{i,j+1} + x_{i,j-1} - 4x_{i,j}] \\
 &\quad + \epsilon_2(1 - \mathcal{G}(\omega))[x_{i+1,j} + x_{i-1,j} + x_{i,j+1} + x_{i,j-1} - 4x_{i,j}], \\
 \dot{y}_{i,j} &= (A - x_{i,j}^2 - y_{i,j}^2)y_{i,j} + \omega_i x_{i,j} - \epsilon_1 \mathcal{G}(\omega)[y_{i+1,j} + y_{i-1,j} + y_{i,j+1} + y_{i,j-1} - 4y_{i,j}] \\
 &\quad + \epsilon_2(1 - \mathcal{G}(\omega))[y_{i+1,j} + y_{i-1,j} + y_{i,j+1} + y_{i,j-1} - 4y_{i,j}].
 \end{aligned} \tag{10}$$

We follow the random discrete distribution for  $\omega_i$  with opposite spins. Based on the value of  $\omega_i$  the interaction between the nearest neighbors is an attractive or level repulsion in a cube. We perform numerical simulations of Eq. (10) in a  $15 \times 15$  grid of Stuart-Landau oscillators. The nonreciprocal interaction induces chimeric patterns in a 2D array, as shown in Fig. 7(a). At  $\epsilon_1 = \epsilon_2 = 0.5$ , Eq. (10) displays a chimera state as shown in Fig. 7(a). We see distinct coherent and incoherent regimes at the surface of the cube. Note that the initial conditions are bipartite. We see that the amplitude of the right half of the cube is considerably less than the left. It is due to the partial distribution in the initial phases, along with randomized  $\omega_i$ . Also, it leads to suppression of oscillations in the  $N/2$  oscillators with the parameter interplay.

We infer that, unlike in the one-dimensional nonreciprocal interactions, 2D arrays are highly correlated according to their initial phases. It causes the definite clustering of oscillators into two distinct regimes. Note that we have interactions in both state variables, unlike in the one-dimensional model. At  $\epsilon_1 = 1.5$  and  $\epsilon = 2$ , we find the coexistence of traveling waves, damped, and coherent oscillations displaying a sort of demonic chimeras, Fig. 7(b). With an increase in coupling strength, the  $+\epsilon$  brings in more harmony and causes traveling waves, while  $-\epsilon$  suppresses the amplitude. The decrement in amplitude results in damped states and small amplitude oscillations. The amplitude response of the overall network is elevated, pivoting an increase in interaction strength due to the strong coupling.

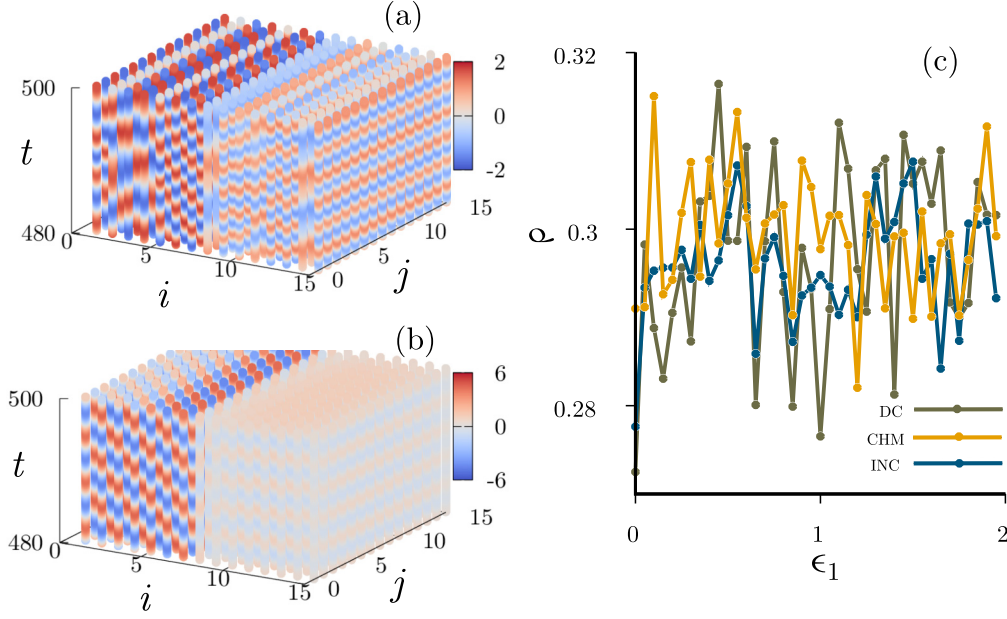


FIG. 7. Chimeric patterns in a 2D array of oscillators with nonreciprocal interactions. (a) Chimera state at  $\epsilon_1 = \epsilon_2 = 0.5$ . (b)  $\epsilon_1 = 1.5$ ,  $\epsilon_2 = 2$ : demonic chimera. (c) Density of coherent oscillators in a unit cube ( $\rho$ ) for three states  $\epsilon_2 = 0.05$ , incoherence;  $\epsilon_2 = 0.5$ , chimeras and  $\epsilon_2 = 0.8$ , demonic chimera.

We also calculate the density  $\rho$  of coherent states based on the autocorrelation of states in a unit cube with the variation in  $\epsilon_1$ . The  $\rho$  is calculated using

$$\rho = \frac{1}{N} C_{ij}(\langle A \rangle), \quad (11)$$

$$C_{ij}(\langle A \rangle) = \begin{cases} 0, & |\langle A_i \rangle - \langle A_j \rangle| < \delta, \\ 1, & |\langle A_i \rangle - \langle A_j \rangle| > \delta. \end{cases} \quad (12)$$

We choose  $\delta = 10^{-3}$  to determine the  $\rho$  of coherent states. We fix  $\epsilon_2 = 0.05$  and vary  $\epsilon_1 \in [0, 2]$ . We see that the incoherent regime follows a low correlation index as  $\epsilon_1$  proceeds, Fig. 7(c). At  $\epsilon_2 = 0.5$ , we detect chimera states. The  $\rho$  follows an increasing trend with the evolution of  $\epsilon_1$ . In the case of demonic chimeras, at  $\epsilon_2 = 0.8$ , we find shuffling of intensities with an increase in  $\epsilon_1$ . It appears due to the presence of traveling waves in the pattern.

## V. CONCLUSION

We study the emergence of chimera states in a network of oscillators with opposite spins. Note that the interaction among the units is nonreciprocal. The interaction switches according to the spin of an oscillator, i.e., clockwise or anti-clockwise. It was found that, due to the spontaneous symmetry breaking of counterrotational symmetry, drifting in spins occur, which causes chimeric patterns. We found that, at the point of transition, exceptional points arise due to the coalescence of eigenvalues. The spectrum of singularities in the parameter space has been estimated numerically. Also, the dynamical restoration of the damped state was preserved because of parity symmetry. Note that the distribution of frequencies is discrete and random. We investigated two cases of initial phases, viz., bipartite and random. In both cases, we found

the appearance of chimeric patterns. Specifically, we noticed an intriguing additional state at the edge of the transition to a damped state, namely, the dDemonic chimera. It is called so because of the coexistence of regular, disordered, and damped regimes. The correlation indices between adjacent nodes are imparted to conceive the dynamical patterns. Moreover, the influence of nonreciprocal interactions is shown in a 2D array of randomly distributed spins. We confirm the appearance of chimera and demonic chimera as in the previous case. This theory will find fruitful application in the fields of metamaterials and optomechanical arrays. Specifically, due to the presence of exceptional points, sensors can be made in the field of photonics.

## ACKNOWLEDGMENT

I acknowledge the anonymous referees for providing useful insights and suggestions that enhance the quality of the manuscript.

## APPENDIX: STUART-LANDAU OSCILLATOR

A pioneer in the school of autonomous oscillators is the Landau-Stuart oscillator that represents an Andronov-Hopf (AH) bifurcation. The AH bifurcation demonstrates the evolution of the limit cycle out of a stable equilibrium. With a change in parameter, a stable origin gets destabilized and gives birth to a stable limit cycle. The LS equation represents the Andronov-Hopf bifurcation and can be written as

$$\dot{z} = -\omega|z|^2 z + \mu z, \quad (A1)$$

where  $z \in \mathbf{C}^N$  and  $\mu, \omega \in \mathbf{C}$ . The  $\mu = \text{Re}(\mu) + i\mu$  and  $\omega = \text{Re}(\omega) + i\omega$  are the parameters determining the distance from the Andronov-Hopf bifurcation and the frequency of



oscillations. The particular case of interest is the  $\text{Re}(\omega) > 0$  or  $\text{Re}(\omega) < 0$ . We know that positive  $\omega$  leads to clockwise rotation of the oscillation and negative  $\omega$  causes anticlockwise oscillation. Also, it is significant to note that at  $\omega = 0$ , the Benjamin-Feir instability causes dispersion of waves. Precisely, the waves of equal and opposite magnitude destabilize each other. It is the significant cause in this study for the manifestation of exceptional points in the eigenplane.

At another perception, the mathematical insight of oscillations is a recurrence of trajectories in the phase space in a small neighborhood of  $\delta$  with an advancement in time. The function  $f(x) := C \mapsto C$  is recurrent in the space  $\delta > 0$ , there exists  $T_\delta > 0$  such that for any  $t \geq 0$  there exists  $T(t, \delta) \in (0, T_\delta)$  such that

$$|x(t + T(t, \delta)) - x(t)| < \delta. \quad (\text{A2})$$

In other words, a recurrent trajectory keeps on passing arbitrarily close to any point and the time intervals between passages through a point and its  $\delta$  vicinity are not necessarily equal but their length cannot grow indefinitely.

The behavior of the system is more clearly demonstrated in polar coordinates. That is, let  $z = \text{Re}^{i\phi}$ , then the equations for the radial amplitude  $r$  and the angular variable  $\phi$  can be decoupled into

$$\begin{aligned} \dot{r} &= \mu r - \omega r^3, \\ \dot{\phi} &= i\mu - i\omega r^2, \end{aligned} \quad (\text{A3})$$

when  $\mu < 0$ , the origin is stable at  $r = 0$ . However,  $\mu > 0$ , the stable fixed point  $r^* = \sqrt{\frac{\mu}{\omega}}$ , when  $r = 0$ , the fixed point becomes unstable. In this case, the initial conditions starting whether from inside or outside converge to a limit cycle of amplitude  $r$ . The  $z(t)$  represents the phase at instant of time in the complex plane and it forms a limit-cycle attractor of amplitude  $\sqrt{\frac{\mu}{\omega}}$ . The bifurcation of the limit cycle from the origin that appears at the value  $\mu = 0$  is known as the Andronov-Hopf bifurcation; the curve defines the limit cycle of the system is given by

$$\Gamma_\alpha = \sqrt{\frac{\mu}{\omega}} \cos(t) + \sqrt{\frac{\mu}{\omega}} \sin(t). \quad (\text{A4})$$

The manifold of Eq. (A3) can be written as

$$\mathcal{W} = \left\{ z \in \mathbb{C} : |z| = \sqrt{\frac{\mu}{\omega}} \right\} \cup \{z = 0\}, \quad (\text{A5})$$

where  $\mathcal{W}$  remains invariant for the trajectories of Eq. (A3). The following theorem generalizes the statement, concerning the case of  $\omega$  and  $\omega_1$ .

*Theorem.* For the unforced Stuart-Landau oscillator, defined by Eq. (A3), the following statements hold true.

- (i) If  $\mu \leq 0$ , the  $z \equiv 0$  is globally exponentially stable.
- (ii) If  $\mu > 0$ , then the limit cycle  $\mathcal{W} = \{z \in \mathbb{C} : |z| = \sqrt{\frac{\mu}{\omega}}\}$  is almost globally asymptotically stable and the origin  $z = 0$  is antistable. Moreover, in this case the oscillation frequency  $\omega$  is defined by  $\omega = i\omega - \frac{i\omega}{\omega} \mu$ .

- 
- [1] M. C. Marchetti, J. F. Joanny, S. Ramaswamy, T. B. Liverpool, J. Prost, M. Rao, and R. A. Simha, *Rev. Mod. Phys.* **85**, 1143 (2013).
  - [2] A. Bricard, J. B. Caussin, N. Desreumaux, O. Dauchot, and D. Bartolo, *Nature (London)* **503**, 95 (2013).
  - [3] F. Ginelli, F. Peruani, M. H. Pillot, H. Chaté, G. Theraulaz, and R. Bon, *Proc. Natl. Acad. Sci.* **112**, 12729 (2015).
  - [4] D. Geyer, A. Morin, and D. Bartolo, *Nat. Mater.* **17**, 789 (2018).
  - [5] N. Bain and D. Bartolo, *Science* **363**, 46 (2019).
  - [6] A. Beer and G. Ariel, *Mov. Ecol.* **7**, 9 (2019).
  - [7] V. Amati, A. Lomi, and A. Mira, *Annu. Rev. Stat. Appl.* **5**, 343 (2018).
  - [8] M. Nagy, Z. Ákos, D. Biro, and T. Vicsek, *Nature (London)* **464**, 890 (2010).
  - [9] A. Cavagna, I. Giardina, and T. S. Grigera, *Phys. Rep.* **728**, 1 (2018).
  - [10] J. Bohannon, *Science* **310**, 219 (2005).
  - [11] T. Carletti and R. Muñoz, *Chaos Solit. Fractals* **164**, 112638 (2022).
  - [12] J. Bascompte, P. Jordano, C. Melián, and J. Olesen, *Proc. Natl. Acad. Sci.* **100**, 9383 (2003).
  - [13] G. Abramson, C. A. Trejo Soto, and L. Ona, *PLoS ONE* **6**, e21028 (2011).
  - [14] Y. Zhang, T. Tsang, E. Bushong, L. Chu, S. Chiang, M. H. Ellisman, J. Reingrubler, and C. Y. Su, *Nat. Commun.* **10**, 1560 (2019).
  - [15] A. Morin, J. B. Caussin, C. Eloy, and D. Bartolo, *Phys. Rev. E* **91**, 012134 (2015).
  - [16] L. L. Bonilla and C. Trenado, *Phys. Rev. E* **99**, 012612 (2019).
  - [17] T. Vicsek, A. Czirók, E. Ben-Jacob, I. Cohen, and O. Shochet, *Phys. Rev. Lett.* **75**, 1226 (1995).
  - [18] A. V. Ivlev, J. Bartnick, M. Heinen, C. R. Du, V. Nosenko, and H. Löwen, *Phys. Rev. X* **5**, 011035 (2015).
  - [19] D. Yllanes, M. Leoni, and M. C. Marchetti, *New J. Phys.* **19**, 103026 (2017).
  - [20] C. Coulais, D. Sounas, and A. Alu, *Nature (London)* **542**, 461 (2017).
  - [21] M. Brandenbourger, X. Locsin, E. Lerner, and C. Coulais, *Nat. Commun.* **10**, 4608 (2019).
  - [22] C. M. Bender, *Rep. Prog. Phys.* **70**, 947 (2007).
  - [23] N. Hatano and D. R. Nelson, *Phys. Rev. Lett.* **77**, 570 (1996).
  - [24] C. M. Bender and S. Boettcher, *Phys. Rev. Lett.* **80**, 5243 (1998).
  - [25] T. Kato, *Perturbation Theory for Linear Operators*, 2nd ed. (Springer, New York, 1984).
  - [26] R. Hanai and P. B. Littlewood, *Phys. Rev. Res.* **2**, 033018 (2020).
  - [27] M. Fruchart, R. Hanai, P. B. Littlewood, and V. Vitelli, *Nature (London)* **592**, 363 (2021).
  - [28] C. Weis, M. Fruchart, R. Hanai, K. Kawagoe, P. B. Littlewood, and V. Vitelli, *arXiv:2207.11667*.
  - [29] M. A. Miri and A. Alù, *Science* **363**, eaar7709 (2019).
  - [30] H. Y. Yuan, R. Lavrijsen, and R. A. Duine, *Phys. Rev. B* **107**, 024418 (2023).

- [31] H. Hong, *Phys. Rev. E* **89**, 062924 (2014).
- [32] F. Parastesh, S. Jafari, H. Azarnoush, Z. Shahriari, Z. Wang, S. Boccaletti, and M. Perc, *Phys. Rep.* **898**, 1 (2021).
- [33] Y. Zhu, Z. Zheng, and J. Yang, *Phys. Rev. E* **89**, 022914 (2014).
- [34] A. Buscarino, M. Frasca, L. V. Gambuzza, and P. Hövel, *Phys. Rev. E* **91**, 022817 (2015).
- [35] E. Schöll, A. Zakharova, and R. G. Andrzejak, *Chimera States in Complex Networks* (Springer, New York, 2020).
- [36] V. Maistrenko, O. Sudakov, and O. Osiv, *Chaos* **30**, 063113 (2020).
- [37] A. Zakharova, M. Kapeller, and E. Schöll, *Phys. Rev. Lett.* **112**, 154101 (2014).
- [38] T. Banerjee, *Europhys. Lett.* **110**, 60003 (2015).
- [39] A. Provata, *Complexity* **1**, 025006 (2020).
- [40] L. Landau, *Dokl. Akad. Nauk SSSR* **44**, 339 (1944).
- [41] J. T. Stuart, *J. Fluid Mech.* **4**, 1 (1958).
- [42] P. G. Drazin and W. H. Reid, *Hydrodynamic Stability* (Cambridge University Press, Cambridge, England, 2004).
- [43] Y. Kuramoto, *Chaos and Statistical Methods* (Springer Science and Business Media, New York, 2012), Vol. 19.
- [44] S. A. M. Loos, J. C. Claussen, E. Schöll, and A. Zakharova, *Phys. Rev. E* **93**, 012209 (2016).
- [45] M. G. Clerc, S. Coulibaly, M. A. Ferré, and M. Tlidi, *Chaos* **30**, 043107 (2020).
- [46] Y. Maistrenko, O. Sudakov, O. Osiv, and V. Maistrenko, *New J. Phys.* **17**, 073037 (2015).
- [47] J. Hizanidis, N. Lazarides, and G. P. Tsironis, *Chaos* **30**, 013115 (2020).
- [48] J. F. Tetz, J. Rode, M. R. Tinsley, K. Showalter, and H. Engel, *Nat. Phys.* **14**, 282 (2018).
- [49] N. Lazarides, G. Neofotistos, and G. P. Tsironis, *Phys. Rev. B* **91**, 054303 (2015).
- [50] X. Huang *et al.*, *J. Neurosci.* **24**, 9897 (2004).
- [51] N. Uchida and R. Golestanian, *Phys. Rev. Lett.* **104**, 178103 (2010).
- [52] A. M. Hagerstrom *et al.*, *Nat. Phys.* **8**, 658 (2012).